Article

Cancer Cell

Long-Pentraxin 3 Derivative as a Small-Molecule FGF Trap for Cancer Therapy

Graphical Abstract

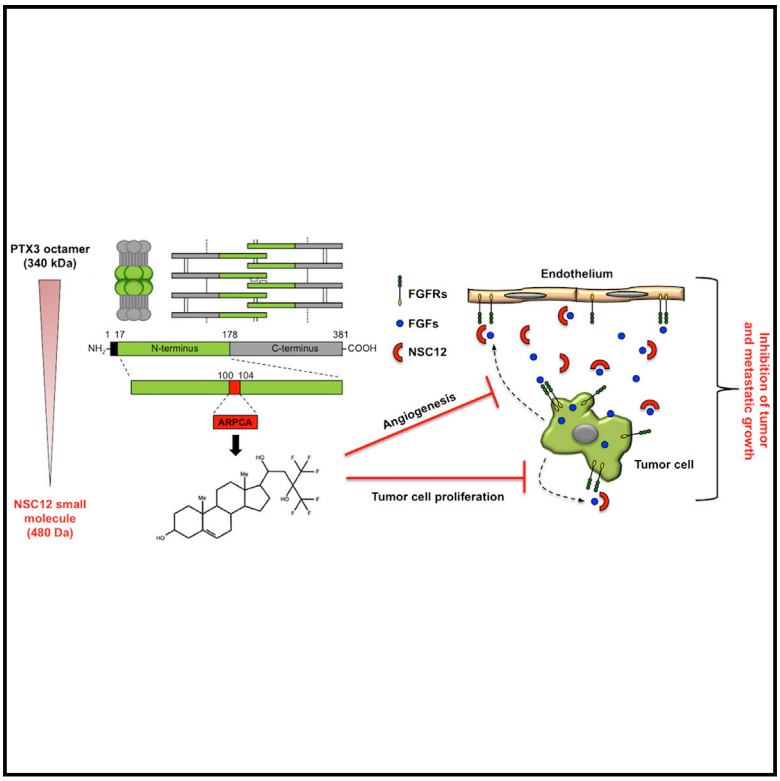

Highlights

- hPTX3 overexpression blocks tumor growth and metastases in transgenic mice
- Pharmacophore modeling identified NSC12 as a PTX3-derived anti-FGF small molecule
- NSC12 inhibits FGF-dependent tumor growth, angiogenesis, and metastases
- NSC12 acts as a small-molecule FGF trap in cancer therapy

Authors

Roberto Ronca, Arianna Giacomini, Emanuela Di Salle, ..., Marco Mor, Giorgio Colombo, Marco Presta

Correspondence

roberto.ronca@unibs.it (R.R.), marco.presta@unibs.it (M.P.)

In Brief

Ronca et al. show that overexpression of long-pentraxin 3 (PTX3) in mice inhibits the growth of FGF-dependent tumor models. On the basis of pharmacophore modeling of PTX3-FGF2 interaction, they identify a small molecule that acts as an extracellular FGF trap and inhibits FGF-dependent tumor growth in mice.

Ronca et al., 2015, Cancer Cell *28*, 225–239
August 10, 2015
http://dx.doi.org/10.1016/j.ccell.2015.07.002

CellPress

Cancer Cell
Article

Long-Pentraxin 3 Derivative as a Small-Molecule FGF Trap for Cancer Therapy

Roberto Ronca,[1,9,*] Arianna Giacomini,[1,9] Emanuela Di Salle,[1] Daniela Coltrini,[1] Katiuscia Pagano,[2] Laura Ragona,[2] Sara Matarazzo,[1] Sara Rezzola,[1] Daniele Maiolo,[3] Rubben Torrella,[4] Elisabetta Moroni,[4] Roberta Mazzieri,[5] Giulia Escobar,[6,7] Marco Mor,[8] Giorgio Colombo,[4,10] and Marco Presta[1,10,*]
[1]Department of Molecular and Translational Medicine, University of Brescia, 25123 Brescia, Italy
[2]NMR Laboratory, Istituto per lo Studio delle Macromolecole, CNR, 20133 Milan, Italy
[3]Chemistry for Technologies Laboratory and INSTM, School of Engineering, University of Brescia, 25123 Brescia, Italy
[4]Istituto di Chimica del Riconoscimento Molecolare, CNR, 20133 Milan, Italy
[5]University of Queensland Diamantina Institute, Translational Research Institute, Brisbane, QLD 4102, Australia
[6]San Raffaele Telethon Institute for Gene Therapy, 20132 Milan, Italy
[7]Vita Salute San Raffaele University, 20132 Milan, Italy
[8]Department of Pharmacy, University of Parma, 43121 Parma, Italy
[9]Co-first author
[10]Co-senior author
*Correspondence: roberto.ronca@unibs.it (R.R.), marco.presta@unibs.it (M.P.)
http://dx.doi.org/10.1016/j.ccell.2015.07.002

SUMMARY

The fibroblast growth factor (FGF)/FGF receptor (FGFR) system plays a crucial role in cancer by affecting tumor growth, angiogenesis, drug resistance, and escape from anti-angiogenic anti-vascular endothelial growth factor therapy. The soluble pattern recognition receptor long-pentraxin 3 (PTX3) acts as a multi-FGF antagonist. Here we demonstrate that human PTX3 overexpression in transgenic mice driven by the *Tie2* promoter inhibits tumor growth, angiogenesis, and metastasis in heterotopic, orthotopic, and autochthonous FGF-dependent tumor models. Using pharmacophore modeling of the interaction of a minimal PTX3-derived FGF-binding pentapeptide with FGF2, we identified a small-molecule chemical (NSC12) that acts as an extracellular FGF trap with significant implications in cancer therapy.

INTRODUCTION

Fibroblast growth factors (FGFs) are heparin-binding polypeptides produced by stromal and parenchymal tumor cells and are readily sequestered into the extracellular matrix by heparan sulfate proteoglycans (HPSGs). FGFs bind tyrosine kinase (TK) FGF receptors (FGFR1–FGFR4), leading to the formation of signaling HSPG/FGF/FGFR ternary complexes (Beenken and Mohammadi, 2009). Activation of the FGF/FGFR system by overexpression, oncogenic mutations, or gene amplifications is implicated in key steps of tumor growth and progression (Beenken and Mohammadi, 2009). Moreover, compensatory upregulation of the FGF/FGFR system may facilitate the escape from angiostatic anti-vascular endothelial growth factor (VEGF) blockade (Casanovas et al., 2005; Lieu et al., 2011). Thus, experimental and clinical evidence provides a compelling biologic rationale for the development of anti-FGF/FGFR targeting agents in cancer therapy.

Thus far two major classes of FGFR inhibitors have been developed: small-molecule intracellular TK inhibitors and extracellular anti-FGFR antibodies or peptides (Ho et al., 2014). However, FGFR redundancy, limited selectivity, and significant toxicity of TK inhibitors and proteinaceous origin of extracellular FGFR antagonists may represent significant challenges for the development of effective anti-cancer drugs. An alternative or complementary approach may derive from the observation that

Significance

The FGF/FGFR system is an attractive target for cancer therapy. To date, only small-molecule inhibitors targeting the tyrosine kinase or extracellular domains of FGFRs have been developed. Here we show that *Tie2* promoter-driven overexpression of human PTX3 in transgenic mice inhibits tumor growth and metastasis in heterotopic, orthotopic, and autochthonous FGF-dependent tumor models. These observations set the basis for pharmacophore modeling and identification of a PTX3-derived small molecule, NSC12, acting as an extracellular FGF trap. Parenteral and oral delivery of NSC12 inhibits FGFR activation, tumor growth, angiogenesis, and metastasis in FGF-dependent murine and human tumor models. NSC12 represents a small-molecule ligand trap that can be developed with therapeutic significance in cancer therapy.

FGFs are highly expressed in certain human tumors and exert paracrine and autocrine functions on cancer epithelial and stromal cells (Brooks et al., 2012), thus providing druggable targets for the development of ''two-compartment'' anti-FGF agents (Dieci et al., 2013), as hypothesized for soluble ''decoy'' FGFRs (Harding et al., 2013; Ho et al., 2014), heparin derivatives, and polysulphated or polysulphonated compounds (Presta et al., 2005). However, the possibility of developing small organic molecules as extracellular multi-FGF ligand traps remains underexplored.

The soluble pattern recognition receptor long pentraxin-3 (PTX3) is produced by endothelial and immune cells in response to inflammatory signals (Garlanda et al., 2005). PTX3 binds various FGFs via its N-terminal extension, including FGF2, FGF6, FGF8b, FGF10, and FGF17, and inhibits FGF-dependent angiogenic responses (Camozzi et al., 2006; Leali et al., 2011; Presta et al., 2007; Ronca et al., 2013a). Accordingly, the acetylated pentapeptide Ac-ARPCA-NH_2 (in single-letter code, hereafter referred to as ARPCA), corresponding to the N-terminal amino acid sequence PTX3(100–104), acts as a minimal anti-angiogenic FGF-binding peptide able to interfere with FGF/FGFR interaction (Leali et al., 2010). Thus, PTX3 represents a natural multi-FGF trap with potential implications for tumor therapy. Indeed, PTX3-overexpressing FGF-dependent tumor cells show a reduced angiogenic and tumorigenic potential (Leali et al., 2011; Ronca et al., 2013a, 2013b).

Here, the effect of endothelial human PTX3 (hPTX3) overexpression on FGF-dependent tumor progression was evaluated in transgenic mice, and pharmacophore modeling was used to identify a PTX3-derived small molecule acting as a FGF trap in cancer therapy.

RESULTS

Generation of Transgenic hPTX3-Expressing TgN(Tie2-hPTX3) Mice

To mimic the effect of a local and systemic delivery of hPTX3 on tumor growth, we generated transgenic TgN(Tie2-hPTX3) mice expressing hPTX3 under the control of the endothelial-specific *Tie2*/*Tek* transcription regulatory sequences. hPTX3 is expressed in various organs of these mice where it accumulates in the perivascular and stromal microenvironment (Figures 1A and 1B), leading to a significant increase of hPTX3 serum levels (105 ± 20 ng/ml versus < 1.8 ng/ml in transgenic and wild-type animals, respectively).

As anticipated, lung endothelial cells isolated from TgN(Tie2-hPTX3) animals showed impaired FGFR1 activation following stimulation by FGF2 when compared to wild-type cells (Figure 1C). In addition, aorta rings harvested from TgN(Tie2-hPTX3) mice and embedded in fibrin gel in the presence of FGF2 showed a reduced capacity to form endothelial cell sprouts but retained a full response to VEGF-A (Figure 1D). Finally, the angiogenic activity of FGF2 was significantly reduced in a subcutaneous (s.c.) Matrigel plug assay performed in TgN(Tie2-hPTX3) animals (Figure 1E). Notably, constitutive hPTX3 expression does not result in apparent defects in embryonic and post-natal development and in body weight gain; adult animals are fertile with no histological alterations of all tissues examined, including heart, liver, lungs, and kidney (data not shown). Moreover, no significant changes in the expression levels of PTX3-targeted FGFs, including *Fgf2*, *Fgf6*, *Fgf8*, *Fgf10*, and *Fgf17* (Ronca et al., 2013a), was observed in different organs of TgN(Tie2-hPTX3) mice when compared to wild-type animals (Figure S1).

Tie2 Promoter-Driven Expression of hPTX3 Impairs Heterotopic Tumor Growth and Neovascularization

Transgenic adenocarcinoma of the mouse prostate (TRAMP)-C2 cells are a prototypic prostate carcinoma model driven by autocrine, androgen-upregulated FGF2 and FGF8b (Ronca et al., 2013a). To assess the impact of hPTX3 overexpression on the early phases of FGF-dependent tumor growth, we performed a short-term experiment in which TRAMP-C2 cells embedded in alginate plugs were injected s.c. in male TgN(Tie2-hPTX3) mice. After 2 weeks, alginate pellets grafted in transgenic animals showed a significant reduction of FGFR1 phosphorylation when compared to plugs implanted in wild-type animals, providing experimental evidence of the capacity of transgenic hPTX3 overexpression to disrupt ligand-dependent FGFR activation in vivo (Figures 2A and 2B). Accordingly, tumor cell proliferation rate and vascularization were drastically impaired in TRAMP-C2 plugs grafted in TgN(Tie2-hPTX3) mice (Figure 2C) with a significant inhibition of TRAMP-C2 tumor growth in a long-term s.c. assay (Figure 2D).

A significant reduction of tumor growth was observed in TgN(Tie2-hPTX3) mice also after s.c. injection of FGF-dependent B16-F10 melanoma cells or Lewis lung carcinoma (LLC) cells, a model in which the FGF/FGFR axis is associated with tumor growth and resistance to anti-VEGF therapy (Figure 2D) (Shojaei et al., 2009). Notably, no difference in the rate of tumor growth occurred in TgN(Tie2-hPTX3) animals grafted with FGF-independent TC-1 or C3 cancer cells (Figure S2A) (Accardi et al., 2014). Similarly, hPTX3 overexpression did not affect the growth of FGFR1-TRAMP-C2 lesions transduced with a constitutively activated form of the intracellular FGFR1 TK domain (Hart et al., 2000) and characterized by a faster rate of growth when compared to parental TRAMP-C2 tumors (Figure S2B).

hPTX3 overexpression inhibited the growth, proliferation rate, and vascularization of experimental liver metastases after intravenous (i.v.) injection of M5076 reticulum cell sarcoma cells (Figures 2E and 2F) (Talmadge and Hart, 1984). A similar inhibition was observed for the growth of B16-F10 melanoma lung metastases (Figures 2G and 2H) that occurred in the absence of any effect of hPTX3 expression on B16-F10 cell homing to the lungs (Figure S2C). In contrast, no difference in lung colonization was observed between wild-type and TgN(Tie2-hPTX3) animals following i.v. injection of FGF-independent TC-1 cells (Figure S2D). Together, these data support the notion that the anti-tumor effect of hPTX3 is related to its extracellular inhibitory action on the autocrine and paracrine loops of stimulation triggered by the FGF/FGFR system in FGF-dependent tumors.

Tie2-expressing monocytes (TEMs), a bone marrow (BM)-derived cell population homing the tumor microenvironment, may act as cell shuttles for a tumor-targeted delivery of anti-cancer therapeutics (De Palma et al., 2007). On this basis, we generated chimeric mice by myelodepletion of wild-type animals followed by reconstitution with the BM harvested from TgN(Tie2-hPTX3) or control GFP-expressing transgenic

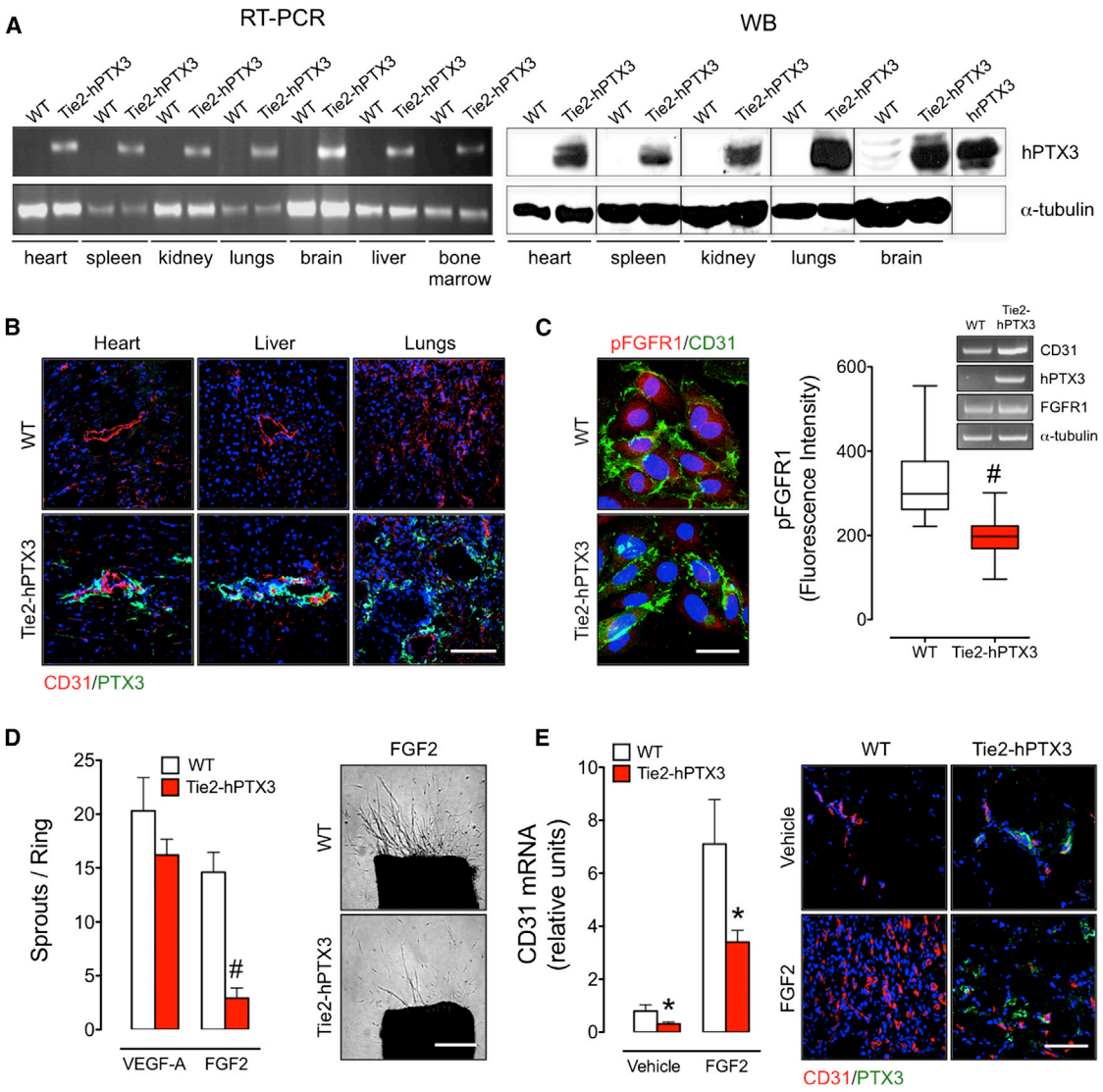

Figure 1. Transgenic TgN(Tie2-hPTX3) Mice

(A) RT-PCR and western blot analyses of the expression of transgenic hPTX3 in wild-type (WT) and TgN(Tie2-hPTX3) mice.

(B) Immunostaining of CD31 (blood vessels) and hPTX3 protein.

(C) Immunostaining for pFGFR1 and CD31 of FGF2-stimulated endothelial cells isolated from WT and TgN(Tie2-hPTX3) lungs. Intensity of pFGFR1 signal was quantified and normalized to DAPI area. The boxes extend from the 25th to the 75th percentiles, lines indicate the median values, and whiskers indicate the range of values. Inset: RT-PCR analysis on isolated cells.

(D) Quantification of the number of sprouts at day 6 and representative images of fibrin-embedded aorta rings from WT and TgN(Tie2-hPTX3) mice treated with FGF2 or VEGF-A.

(E) qRT-PCR (n = 8 mice/group) and immunofluorescence analyses of CD31 expression in vehicle and FGF2 Matrigel plugs.

Scale bars, 50 μm (B and E), 30 μm (C), and 400 μm (D). Data are mean ± SEM. *p < 0.05, and #p < 0.001. See also Figure S1.

TgN(Tie2-GFP) mice (Figures S2E and S2F). As shown in Figure 2I, myeloid-cell-mediated delivery of hPTX3 by TEMs infiltrating the s.c. TRAMP-C2 tumors (Figure S2G) caused a significant delay of tumor growth in chimeric TgN(Tie2-hPTX3) BM-transplanted mice when compared with tumors grafted in TgN(Tie2-GFP) BM-transplanted animals. The inhibitory effect was paralleled by a significant reduction of tumor cell proliferation, but not of tumor vascularization (Figures S2H and S2I), possibly as a consequence of the lower local and systemic concentration of hPTX3 produced by transplanted myeloid cells compared to hPTX3 transgenic animals.

Tie2 Promoter-Driven hPTX3 Production Impairs Orthotopic and Autochthonous Multistage Tumor Growth

Next, we evaluated the effect of stroma-derived hPTX3 on the growth of syngeneic murine pancreatic and mammary carcinoma cells orthotopically grafted in TgN(Tie2-hPTX3) mice.

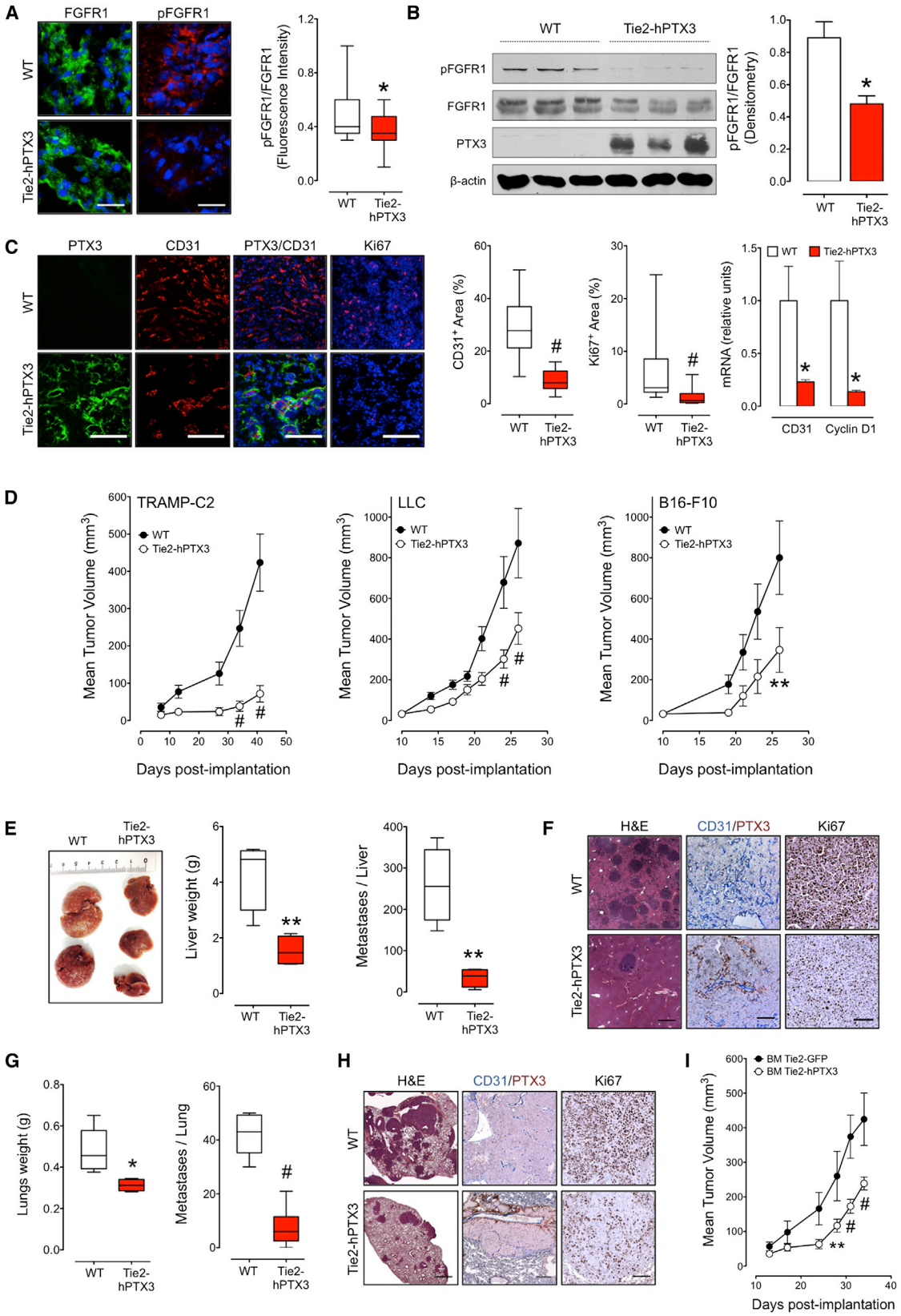

(legend on next page)

When compared to wild-type animals, intra-pancreatic injection of Panc02 tumor cells in TgN(Tie2-hPTX3) mice resulted in a significant reduction of tumor burden and enhancement of animal survival (Figure 3A). Similarly, a significant delay in the appearance of mammary tumor nodules, decreased tumor growth, and increased survival time were observed in female TgN(Tie2-hPTX3) mice with respect to control animals after transplantation of syngeneic EO771 breast carcinoma cells into the mammary fat pad (Figure 3B).

TRAMP mice represent an autochthonous multistage model of prostate cancer in which the FGF/FGFR system plays a relevant role (Polnaszek et al., 2003). To further assess the anti-neoplastic potential of the FGF trap activity of hPTX3, the prostatic tumor progression in double-transgenic TgN(Tie2-hPTX3)/TRAMP mice was compared to the progression in age-matched TRAMP animals at 10 and 12 weeks of age. Quantitative histological analysis revealed a lower incidence of well-differentiated and moderately differentiated tumors (Figure 3C) and a reduction of $Ki67^+$ tumor cells (Figure 3D) in TgN(Tie2-hPTX3)/TRAMP mice, index of significant delay of prostatic tumor progression in hPTX3-expressing mice. This effect was transient and was not observed at later stages of tumor progression in which poorly differentiated or neuroendocrine tumors arose (data not shown), possibly due to compensatory mechanisms that overcome FGF inhibition by PTX3. Even though further experiments will be required to assess the mechanisms able to overcome PTX3-mediated oncosuppressive effects, the data clearly show that PTX3 can delay, at least transiently, the progression of prostate cancer in the TRAMP model.

Homozygous *Ptx3* Inactivation Enhances FGF-Dependent Angiogenesis, Tumor Growth, and Metastasis

$Ptx3^{-/-}$ mice develop normally and do not show any gross abnormality, even though $Ptx3^{-/-}$ females are subfertile. PTX3 deficiency causes a reduced immune response to pathogens and increases tissue damage in ischemic myocardium and atherosclerotic lesions (see Daigo et al. [2014] for a more detailed description of the $Ptx3^{-/-}$ mouse phenotype). Also, recent observations have shown that the growth of chemical carcinogen-induced skin tumors is delayed in these animals (Bonavita et al., 2015). To further evaluate the impact of PTX3 on tumor growth, we compared the angiogenic activity of FGF2 protein and the tumorigenic and metastatic activity of melanoma B16-F10 cells when assessed in syngeneic $Ptx3^{-/-}$ mice versus wild-type and TgN(Tie2-hPTX3) animals. As shown in Figure 3E, *Ptx3* knockout results in a significant increase of both basal and FGF2-triggered angiogenic responses in the Matrigel plug assay when compared to those observed in TgN(Tie2-hPTX3) and wild-type animals. It must be pointed out that the s.c. injection of Matrigel induces per se a mild pro-inflammatory reaction, leading to the co-expression within the plug of PTX3 and FGF2, thus explaining the effect of *Ptx3* knockout on the basal neovascular response in this assay (Leali et al., 2012). In agreement with these observations, the tumorigenic and metastatic activities of B16-F10 cells were significantly enhanced in *Ptx3* null animals in respect to wild-type and hPTX3-overexpressing mice (Figures 3F and 3G). Thus, PTX3 appears to act as a natural brake of FGF-mediated angiogenesis, tumor growth, and metastasis. This inhibitory activity is further enhanced by *Tie2* promoter-driven hPTX3 overexpression in tumor-bearing mice. These observations paved the way for the exploitation of the FGF trap activity of PTX3 in cancer therapy and for the development of PTX3-derived anti-FGF synthetic compounds.

Identification of a PTX3-Derived Small-Molecule FGF Trap

PTX3 is a 340-kDa protein composed of eight protomers of 381 amino acids each (Inforzato et al., 2010). The complex proteinaceous structure of PTX3 hampers its pharmacological exploitation. In this context, we identified the acetylated pentapeptide PTX3(100–104) ARPCA as the minimal amino acid sequence able to bind FGF2 and interfere with FGF2/PTX3 and HSPG/FGF2/FGFR1 interactions (Leali et al., 2010). ARPCA acts as a potent FGF2 and FGF8b antagonist (Leali et al., 2010; Ronca et al., 2013a; Giacomini et al., 2015), representing a useful starting point for the rational identification of low-molecular-weight, nonpeptidic FGF antagonists.

On this basis, an atomistic model of the ARPCA/FGF2 complex was generated to identify the physico-chemical determinants required for productive ARPCA/FGF2 interaction. This information was translated into a pharmacophore model for the identification of drug-like hits via the screening of small-molecule libraries (Colombo et al., 2010). First, the principal conformations populated by ARPCA in solution, derived from a 200-ns-long explicit water molecular dynamics (MD) simulation, were subjected to multiple docking runs on the FGF2 surface, followed by MD refinement of the resulting complex (~100 ns). The results (detailed in the Supplemental Information) showed that ARPCA engages the FGF2 surface that faces the D2-D3 linker and D3 domain of FGFR (Plotnikov et al., 1999). The analysis of the statistical distribution of ARPCA/FGF2 interactions was consistent

Figure 2. Transgenic *hPTX3* Expression Impairs Heterotopic Tumor Growth

(A) FGFR1 and pFGFR1 immunostaining and pFGFR1/FGFR quantification normalized to DAPI area.

(B) Western blot analysis and pFGFR1/FGFR1 quantification normalized to β-actin.

(C) PTX3, CD31, and Ki67 immunostaining, $CD31^+$ and $Ki67^+$ quantification normalized to DAPI area, and relative levels of CD31 and cyclin D1 mRNA expression normalized to 18S rRNA. Eight to ten mice/group in (A)–(C).

(D) Growth of s.c. TRAMP-C2, LLC, and B16-F10 tumors in WT and TgN(Tie2-hPTX3) mice (n = 10–12 mice/group).

(E–H) M5076 (E and F) and B16-F10 (G and H) cells were injected i.v. in WT and TgN(Tie2-hPTX3) mice (n = 10 mice/group). After 3 weeks, liver (E) and lungs (G) were weighed, and macroscopic metastases were counted. Liver (F) and lungs (H) were H&E stained, double-immunostained for CD31/PTX3, and immunostained for Ki67.

(I) Growth of s.c. TRAMP-C2 tumors in WT chimeric mice reconstituted with TgN(Tie2-hPTX3) or control TgN(Tie2-GFP) bone marrow (BM); n = 10 mice/group. Scale bars, 30 μm (A), 100 μm (F [CD31/PTX3 and Ki67], H [Ki67]), 200 μm (H [CD31/PTX3]), and 400 μm (F and H [H&E]). Data are mean ± SEM. In box and whiskers graphs, boxes extend from the 25th to the 75th percentiles, lines indicate the median values, and whiskers indicate the range of values. *$p < 0.05$, **$p < 0.01$, and #$p < 0.001$. See also Figure S2.

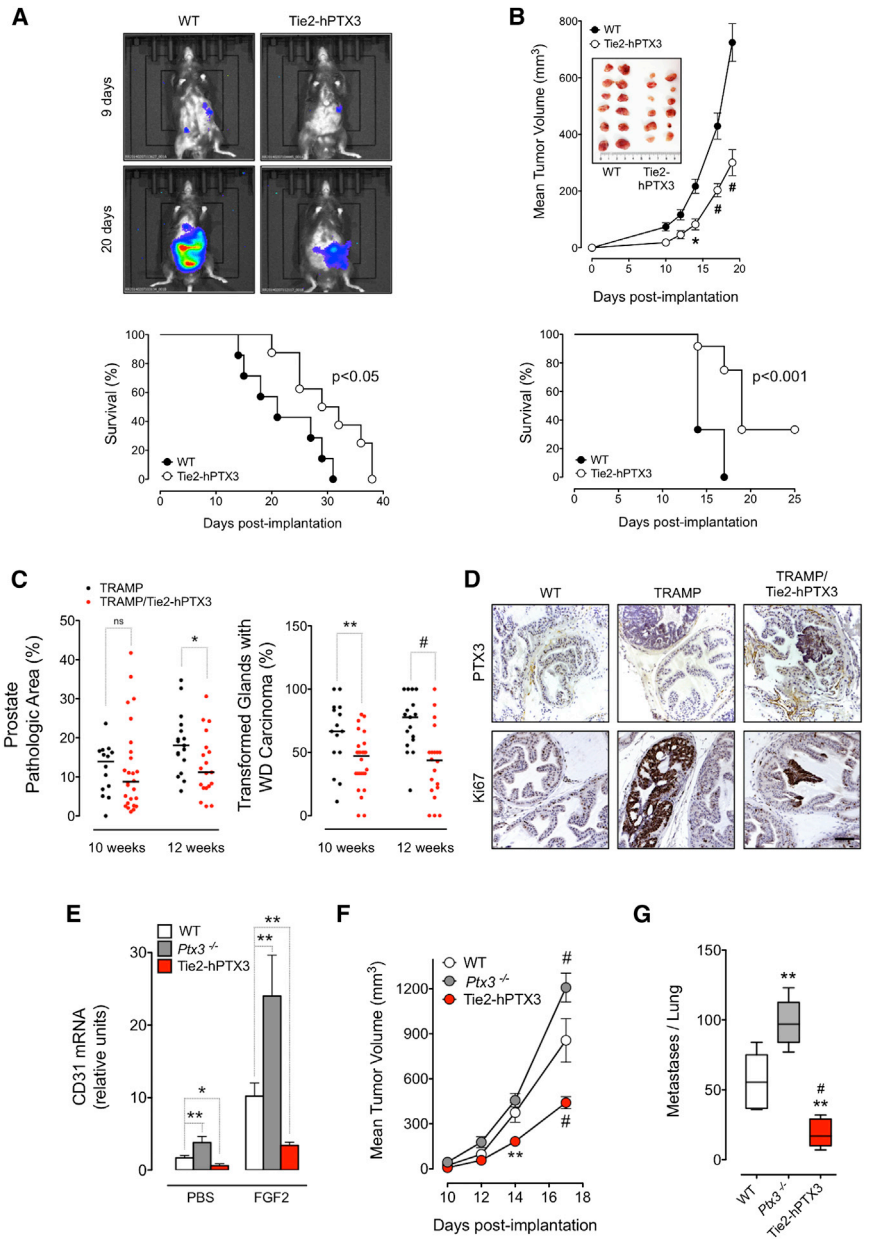

Figure 3. Transgenic hPTX3 Expression Impairs Orthotopic and Multistage Tumor Growth

(A) Imaging of Panc02-*luc* prostate cancer cells 9 and 20 days after orthotopic injection in WT and TgN(Tie2-hPTX3) mice (top panel) and Kaplan-Meyer survival curves (n = 8–10 mice/group) (bottom panel).

(B) Tumor growth, harvested tumors (top panel), and Kaplan-Meyer survival curves (bottom panel) for EO771 mammary carcinoma grafts (n = 10 mice/group).

(C) Histopathological analysis of anterior prostate lobes from 10- and 12-weeks-old TRAMP and TRAMP/Tie2-hPTX3 mice (n = 8–12 mice/group). Left graph shows the percentage of pathologic area on total prostatic area; right graph shows the percentage of pathologic glands with well-differentiated (WD) carcinoma areas. Each dot represents a single tissue field, and lines indicate the median values.

(D) Representative images of anterior prostate sections. Scale bar, 100 μm.

(E–G) qRT-PCR analysis of CD31 expression in PBS and FGF2 Matrigel plugs (E), growth of s.c. B16-F10 tumors (n = 10 mice/group) (F), and quantification of B16-F10 end-stage lung metastatic foci (G) in *Ptx3*$^{-/-}$, WT, and Tie2-hPTX3 mice.

Data are mean ± SEM. The boxes extend from the 25th to the 75th percentiles, lines indicate the median values, and whiskers indicate the range of values. *p < 0.05, **p < 0.01, #p < 0.001, and ns = not significant.

with previously published nuclear magnetic resonance (NMR) saturation-transfer difference (STD) data, indicating that the peptide contacts FGF2 via the methyl groups of Ala1 and Ala5 and of the acetyl capping group (Leali et al., 2010). Next, the ARPCA key functional groups, combined with the characterization of their relative space orientations, were used to build a pharmacophore model for the screening of the NCI2003 small-molecule database containing ~3 × 10^5 compounds (Developmental Therapeutics Program NCI/NIH at https://dtp.cancer.gov/).

Filtering of the resulting set according to the Lipinsky drug-likeness rules returned 25 compounds. Ten of them, made available from the National Cancer Institute (NCI), were subjected to a preliminary screening for their capacity to prevent the formation of HSPG/FGF2/FGFR1(IIIc) ternary complexes in a FGF2-mediated cell-cell adhesion assay. This assay is based on the capacity of FGFs to interact simultaneously in *trans* with HSPGs and FGFRs expressed on neighboring cells, thus causing FGF-mediated cell-cell adhesion (Richard et al., 1995); FGF antagonists hamper FGF-mediated intercellular adhesion by binding FGF and preventing its interaction with HSPGs or FGFRs (Leali et al., 2010). As shown in Figure S3A, the 480-Da compound 4,4,4-trifluoro-1-(3-hydroxy-10,13-dimethyl-2,3,4,7,8,9,11,12,14,15,16,17-dodecahydro-1H-cyclopenta[a]phenanthren-17-yl)-3-(trifluoromethyl) butane-1,3-diol (NSC172285, herewith named NSC12; Figure 4A) prevented the formation of the HSPG/FGF2/FGFR1 complex (half maximal inhibitory concentration (IC_{50}) ~10 μM; Figure 4B), whereas the other compounds were devoid of significant activity. On this basis, NSC12 was characterized further, and the NSC21 compound was used as a negative control.

In a first set of experiments, NSC12 was investigated by surface plasmon resonance (SPR) analysis for its capacity to prevent the binding of FGF2 to heparin immobilized to a BIAcore sensor chip or to an immobilized sFGFR1(IIIc)/Fc chimera. As shown in Figure 4C, NSC12 does not affect FGF2/heparin interaction, whereas it inhibits the binding of FGF2 to the

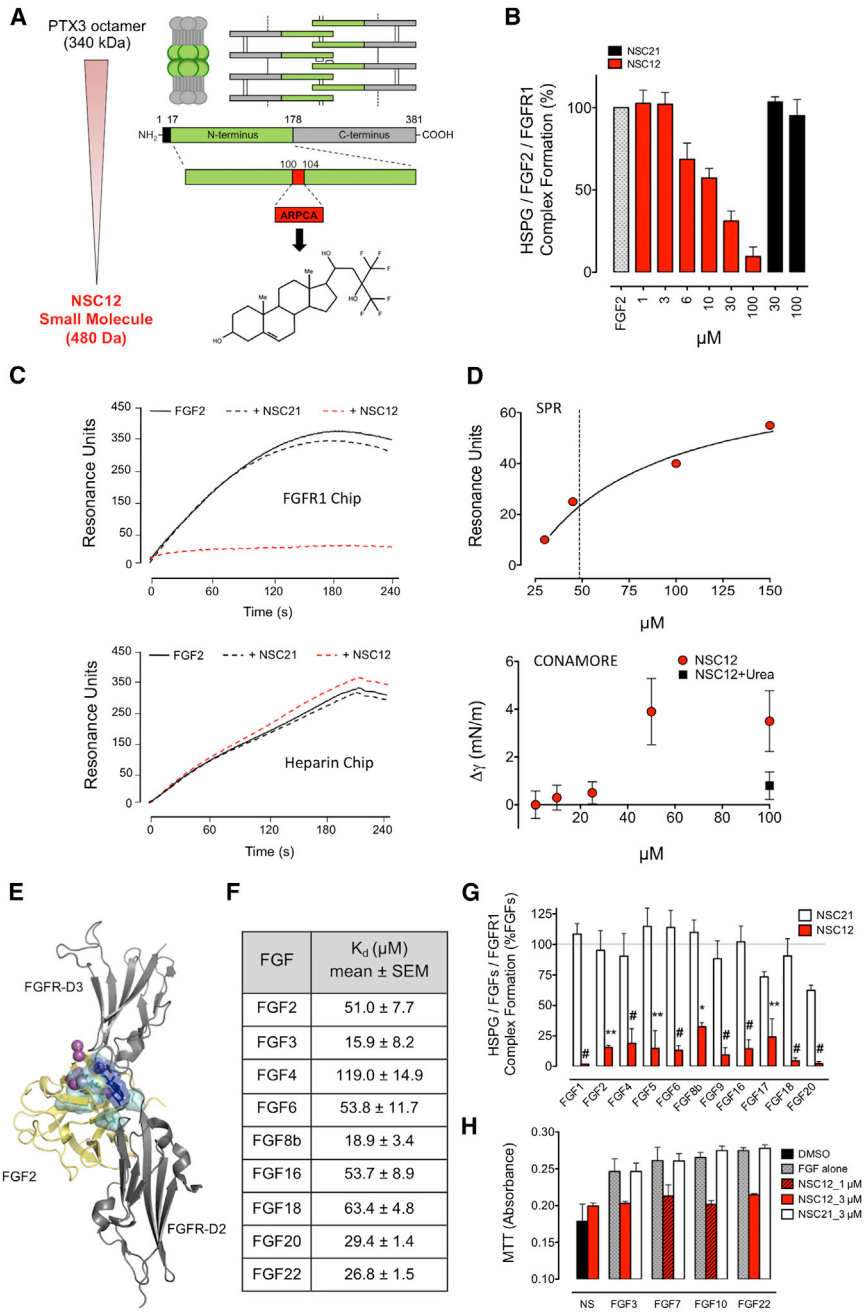

FGF	K_d (μM) mean ± SEM
FGF2	51.0 ± 7.7
FGF3	15.9 ± 8.2
FGF4	119.0 ± 14.9
FGF6	53.8 ± 11.7
FGF8b	18.9 ± 3.4
FGF16	53.7 ± 8.9
FGF18	63.4 ± 4.8
FGF20	29.4 ± 1.4
FGF22	26.8 ± 1.5

Figure 4. NSC12 as a Small-Molecule PTX3-Derived FGF Trap

(A) Schematic representation of multimeric PTX3 protein, highlighting the N-terminal FGF-binding region ARPCA, and chemical structure of NSC12.

(B) Inhibition of HSPG/FGF2/FGFR1 ternary complex formation by NSC12.

(C) SPR competition assay for FGF2 binding to FGFR1 and heparin sensor chips in the presence of 100 μM NSC12 or NSC21.

(D) SPR and CONAMORE analysis of NSC12 affinity and binding on FGF2 sensor chip.

(E) Representation of the main binding mode of NSC12 predicted by docking and MD simulation of NSC12/FGF2 complex. NSC12 and the FGF2 side chains in contact with NSC12 are shown as blue and cyan sticks, respectively, whereas FGF2 and FGFR (PDB ID 1fq9) are shown as yellow and gray cartoons, respectively. Magenta spheres refer to FGF2 residues involved in ARPCA interactions as deduced by MD simulations.

(F) Affinity (K_d) of NSC12/FGF interactions assessed by SPR.

(G and H) NSC12 inhibits HSPG/FGF/FGFR1 ternary complex formation by FGFR1(IIIc)-binding FGFs (G) and MMT-assessed KATO III cell proliferation triggered by FGFR2(IIIb)-binding FGFs (H). Data are mean ± SEM. NS, not stimulated. *$p < 0.05$, **$p < 0.01$, and #$p < 0.001$. See also Figure S3.

immobilized receptor (ID_{50} ~30 μM). No effect was exerted by NSC21 on either sensor chip. Thus, as observed for PTX3/FGF2 and ARPCA/FGF2 complexes (Leali et al., 2010), NSC12 interferes with FGF2/FGFR1 interaction without affecting the ability of the growth factor to interact with heparin or HSPGs.

The capacity of NSC12 to bind to immobilized FGF2 was confirmed by SPR spectroscopy. The SPR binding isotherm (Figure 4D) shows a Langmuir-like shape for monovalent binding with a dissociation constant (K_d) equal to 51 ± 7 μM. The 1:1 stoichiometry of the FGF2:NSC12 interaction was confirmed also by surface density SPR measurements (Maiolo et al., 2012) performed at 100 μM NSC12 and showing that 1.28×10^{10} molecules/mm^2 of NSC12 bind to 1.45×10^{10} molecules/mm^2 of immobilized FGF2.

FGF2/NSC12 interaction was investigated also by the contact angle molecular recognition (CONAMORE) biosensor that probes the nanomechanical aspects of binding, complementing the information obtained by SPR (Maiolo et al., 2012). The CONAMORE binding isotherm performed on the same FGF2 chip used for SPR (Figure 4D) evidences that the onset of significant nanomechanical effects of FGF2 binding occurs at ~40 μM NSC12, consistent with the K_d calculated by SPR. In addition, no nanomechanical effect is registered when NSC12 is run onto a urea-denatured FGF2 chip (Figure 4D), further pointing to the specificity of the interaction.

Docking and MD simulations performed on the NSC12/FGF2 system indicated that NSC12 and ARPCA, while sharing the same pharmacophoric points necessary to anchor FGF2, do not target entirely identical or overlapping regions on the FGF2 molecule, as expected given their different chemical nature and pharmacophore design. Indeed, besides engaging the FGF2 surface that faces the D2-D3 linker and D3 domain of FGFR, NSC12 further extends into the FGF2 region facing the FGFR D2 domain (D2), as detailed in the Supplemental Information and in Figure 4E. On this basis and given that the D3 domain

does not adopt a stable persistent three-dimensional fold in solution (Herbert et al., 2013), the D2 domain was used as a probe to investigate the overall effects of NSC12 on the FGF2/FGFR complex by NMR. Relaxation data demonstrate that NSC12 shifts the FGF2/D2 equilibrium toward the uncomplexed forms, as deduced from the decrease of the average ^{15}N transverse relaxation rate value measured for D2 and FGF2 upon NSC12 addition to the D2/FGF2 complex (Supplemental Information and Figure S3B).

Finally, when tested by SPR analysis on all canonical FGFs (Itoh and Ornitz, 2004), NSC12 also binds immobilized FGF3, FGF4, FGF6, FGF8, FGF16, FGF18, FGF20, and FGF22 with K_d values ranging between ~16 and ~120 μM (Figure 4F). No apparent interaction was observed for the other FGFs tested, possibly because of the limited sensitivity of the method due to the low molecular weight of NSC12 or to the low efficiency of the immobilization procedure for some of the FGFs tested. On this basis, the capacity of NSC12 to affect the activity of FGFR1(IIIc)-binding FGFs and of FGFR2(IIIb)-binding FGFs (Zhang et al., 2006) was assessed by the HSPG/FGF/FGFR1 ternary complex assay described above and by a KATO III cell proliferation methylthiazol tetrazolium (MTT) assay (Bai et al., 2010), respectively. As shown in Figures 4G and 4H, NSC12 inhibits HSPG/FGF/FGFR ternary complex formation induced by FGFR1(IIIc)-binding FGF1, FGF4, FGF5, FGF6, FGF8, FGF9, FGF16, FGF17, FGF18, and FGF20 and the proliferative capacity of FGFR2(IIIb)-binding FGF3, FGF7, FGF10, and FGF22 in KATO III cells. Together with its FGF2 antagonist activity, these data indicate that NSC12 may act as a multi-FGF trap by interacting with all members of the canonical FGF subfamilies. In addition, when assessed for its ability to interact with hormonal FGFs, SPR analysis showed the capacity of NSC12 to bind FGF21 (K_d = 53 ± 13 μM) but failed to detect a significant interaction with immobilized FGF19 or FGF23. However, when tested on MDA-MB-361 breast cancer cells, the compound was able to inhibit $ERK_{1/2}$ phosphorylation and the mitogenic response elicited by all hormonal FGFs in these cells (Figure S3C). Accordingly, NSC12 hampered FGF23-mediated FGFR1 activation in Klotho-expressing Chinese hamster ovary (CHO) cells (Figure S3D) (Urakawa et al., 2006).

NSC12 Inhibits FGF-Dependent Angiogenesis and Tumor Cell Proliferation

In keeping with its capacity to antagonize FGF2/FGFR1 interaction, NSC12 inhibited FGFR1 phosphorylation in human umbilical vein endothelial cells (HUVECs) stimulated by FGF2 with a significant inhibition of HUVEC proliferation (IC_{50} ~6.5 μM) mainly due to their accumulation in the G_0/G_1 phase of the cell cycle (Figures 5A and 5B). Also, NSC12 inhibited the sprouting activity exerted by FGF2 on HUVEC spheroids embedded in fibrin gel (Figure 5C) and impaired the angiogenic response triggered by FGF2 in the chick embryo chorioallantoic membrane (CAM) assay (Figure 5D). NSC12 had no effect on the activity of VEGF-A in all these assays, and control NSC21 was inactive. Thus, NSC12 acts as a selective anti-angiogenic FGF antagonist. Accordingly, the inhibitory activity exerted by NSC12 on endothelial cell proliferation, as well as on tumor cell proliferation (see below), was reversed by a molar excess of FGF2 (Figure S4A).

When challenged in vitro on tumor cell lines, NSC12 impaired the FGF-mediated proliferation of murine (TRAMP-C2) and human (LNCaP and DU145) prostate cancer cells where FGFR1 is a driver of tumor growth and drug resistance (Figure 5E). Similar results were obtained for FGF-dependent murine (LLC) and human (H520) lung cancer cells characterized by *FGFR1* overexpression or amplification, respectively (Figure 5F). As observed for HUVECs, treatment with NSC12 caused the reduction of the S phase of the cell cycle in all tumor cell lines but LLC cells, in which an accumulation in the S phase was observed (Figures 5E and 5F). Control NSC21 was inactive in all the cell lines tested, and no inhibitory effect was observed when FGF/FGFR-independent HCC827 lung cancer cells (harboring a tumor-driving mutation of the epidermal growth factor receptor [EGFR] TK domain) were challenged with NSC12 (Figure 5F).

The inhibitory activity of NSC12 was not restricted to FGFR1-dependent tumor cells. Indeed, the compound also affected the proliferation of FGFR2-dependent KATO III gastric carcinoma cells, FGFR3-dependent KMS-11 myeloma cells, and FGFR4-dependent MDA-MB-361 breast cancer cells (Figure S4B). Accordingly, NSC12 inhibited FGFR1, FGFR2, FGFR3, and FGFR4 phosphorylation in CHO cell transfectants (Figure S4C).

To define a therapeutically effective dose and to assess the FGF antagonist activity of NSC12 in vivo, TRAMP-C2 cells were embedded in alginate plugs and grafted s.c. in syngeneic male mice that were treated intraperitoneally (i.p.) every other day for 1 week with increasing doses of NSC12 (from 2.5 to 10 mg/kg). NSC12 caused a significant decrease of tumor weight, tumor cell FGFR1 phosphorylation and proliferation, and tumor $CD31^+$ neovascularization at all the doses tested, whereas NSC21 was ineffective (Figures 6A–6C and S5A). Since the 10-mg/kg dose resulted in a partial body weight loss (Figure S5B), the 7.5-mg/kg dose was chosen for further experimentation. This dose was sufficient to fully inhibit FGFR1 phosphorylation in TRAMP-C2/alginate implants (Figure 6D) with no effect in 2-week-treated animals on body weight (Figure S5B), hematologic parameters, and blood serum components (Figure S5C). Remarkably, NSC12 treatment did not affect serum concentration of endocrine FGFs, including FGF23 (Figure S5D).

On this basis, additional short-term assays were performed on FGF-dependent human cancer cells. To this aim, alginate plugs containing human prostate cancer (DU145) or lung cancer (H520) cells were injected s.c. in immunodeficient mice that were treated i.p. every other day with 7.5 mg/kg NSC12 or NSC21 for 1 week. As shown in Figures 6E and 6F, NSC12 caused a significant reduction of tumor weight and tumor $CD31^+$ neovascularization with a consequent increase of tumor cell death (as assessed by TUNEL staining). Notably, in keeping with in vitro observations, i.p. administration of NSC12 did not exert any effect in vivo on FGF-independent HCC827 tumor cells, causing only a limited inhibition of the scarce neovascular response elicited by these cells (Figure 6G). Again, NSC21 was ineffective in all the alginate plugs tested.

Together, these data provide strong experimental evidence about the capacity of a small-molecule FGF trap to disrupt FGF/FGFR signaling in vivo, leading to inhibition of tumor cell proliferation and neovascularization in FGF-dependent tumors.

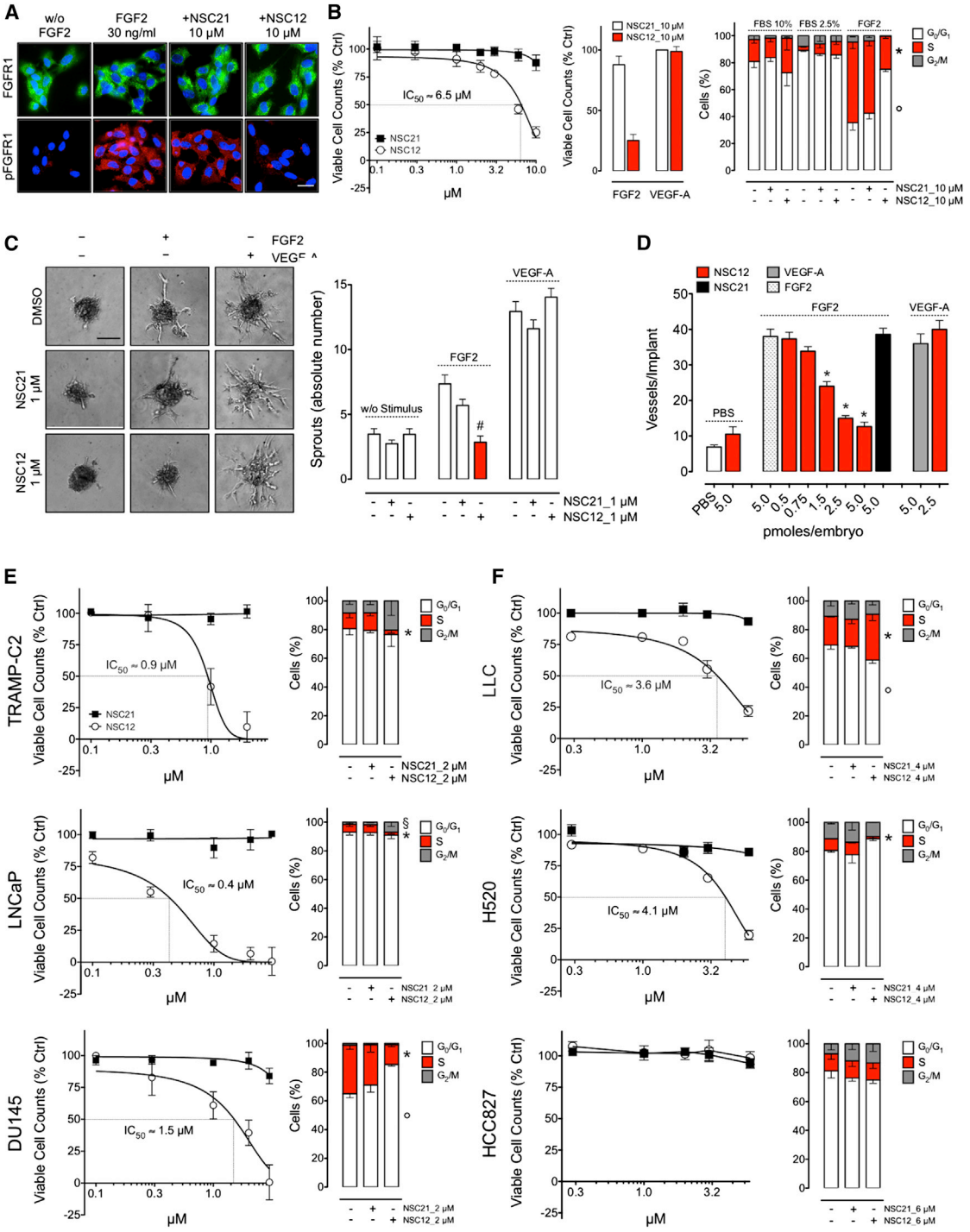

Figure 5. In Vitro Anti-tumor Effects of NSC12

(A and B) FGFR1 and pFGFR1 immunostaining (A), viable cell counting, and cell cycle analysis (B) of HUVE cells treated with FGF2, VEGF-A, or FBS in the presence of NSC12 or NSC21.

(C) HUVE cell spheroids were stimulated with FGF2 or VEGF-A in the absence or presence of 1.0 μM NSC12 or NSC21. After 24 hr, the number of sprouts or spheroids were counted.

(D) FGF2 and VEGF-A alginate pellets were placed on top of the chick embryo CAM at day 11 in the absence or presence of NSC12 or NSC21. At day 14 blood vessels around the sponges were counted (n = 8 eggs/group).

(E and F) Viable cell counting and cell cycle analysis of prostate cancer cells (E) and lung cancer cells (F).

*$p < 0.05$, and #$p < 0.001$. Scale bars, 20 μm (A) and 100 μm (C). Data are mean ± SEM. For cell cycle analyses: $p < 0.01$, *S phase, $^{\circ}G_0/G_1$ phase, and $^{\S}G_2/M$ phase. See also Figure S4.

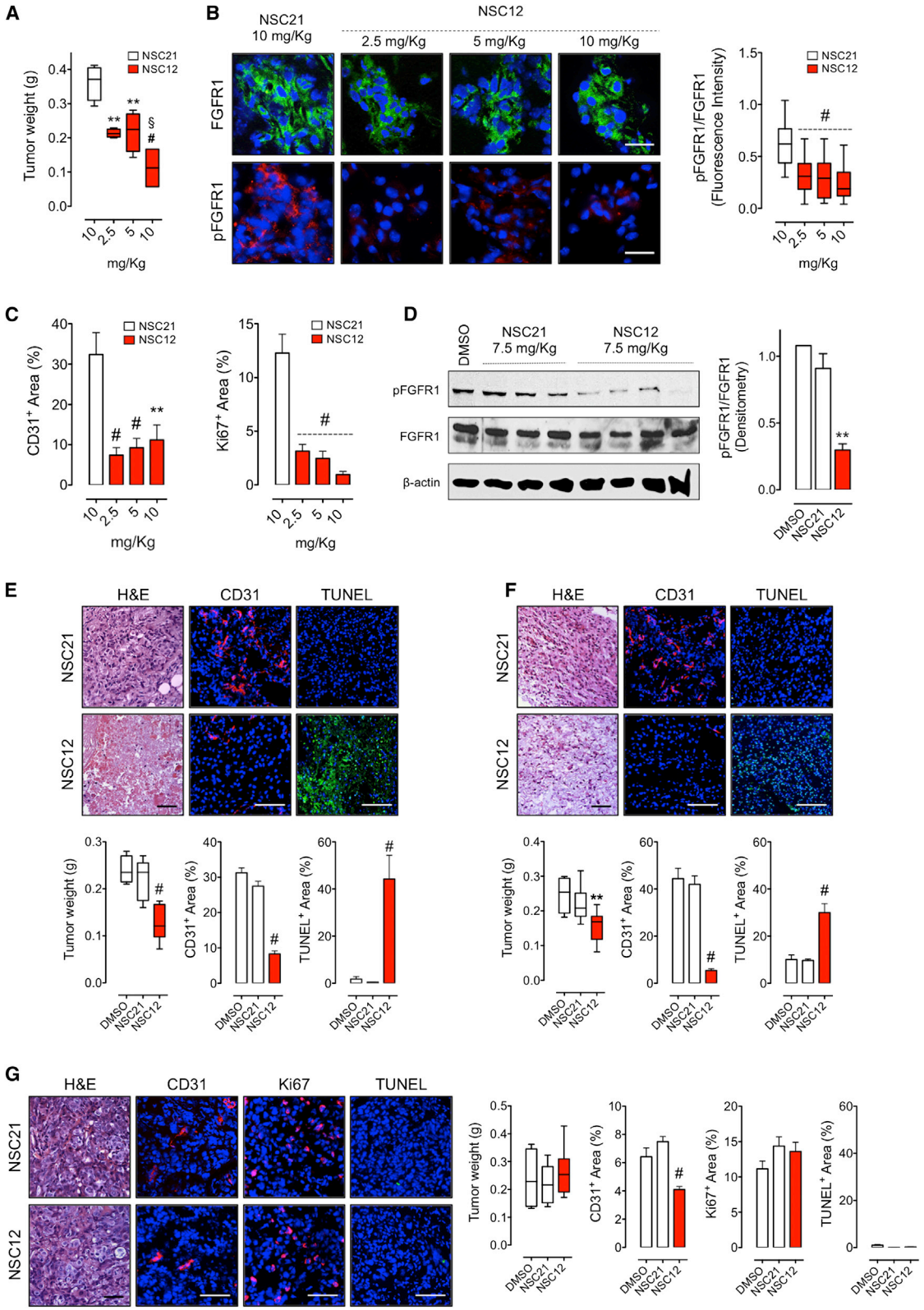

Figure 6. NSC12 Inhibits the FGF/FGFR System in FGF-Dependent Tumors

(A–D) Male mice were implanted s.c. with TRAMP-C2/alginate plugs and treated i.p. every other day with NSC12, NSC21, or vehicle (n = 4–6 mice/group). After 1 week, harvested plugs were weighed (A), processed for immunofluorescence analysis of FGFR1 and pFGFR1 (B) or of CD31and Ki67 (C) or for pFGFR1/FGFR1 quantification by western blot analysis of FGFR1 and pFGFR1 (data are normalized to β-actin; D).

(legend continued on next page)

Inhibition of Tumor Growth by Parenteral and Oral Delivery of NSC12

On the basis of results described above, NSC12 was assessed for its capacity to inhibit the tumorigenic activity of FGF-dependent TRAMP-C2 cells and of human prostate DU145 and lung H520 tumor cells following i.p. administration in syngeneic and nude mice, respectively. To this purpose, tumor cells were injected s.c., and animals were randomly distributed in vehicle-, NSC12-, or NSC21-treated groups when tumors were palpable. As shown in Figure 7A, NSC12 exerted a significant inhibitory effect on the growth of both murine and human tumor grafts, whereas NSC21 was ineffective. Moreover, NSC12 inhibited the formation of experimental lung metastases after i.v. injection of B16-F10-*luc* cells (Figure 7B) and of spontaneous lung metastases induced by orthotopic grafting of breast carcinoma EO771 cells into the mammary fat pad followed by surgical removal of the primary tumor (Figure 7C). In contrast, NSC12 did not affect the growth of FGF-independent TC-1 and C3 tumor grafts or of TRAMP-C2 and LLC lesions overexpressing the constitutively activated form of the intracellular FGFR1 TK domain, thus confirming the specificity of the effect (Figure S6).

Finally, to establish whether NSC12 may also exert a significant anti-tumor activity after oral administration, male mice were injected s.c. with TRAMP-C2 cells embedded in alginate plugs and treated by gavage with 7.5 mg/kg NSC12 or NSC21 for 4 days. Strikingly, gavage administration of NSC12 significantly impaired FGFR1 phosphorylation in TRAMP-C2 plugs when compared to plugs from animals treated with NSC21 or vehicle (Figure 7D). To confirm the oral activity of NSC12 also in human tumors, FGF-dependent H520 cells were grafted s.c. in nude mice. When tumors were palpable, animals were randomly distributed in three experimental groups and treated orally with 7.5 mg/kg NSC12 or NSC21 or vehicle. As shown in Figure 7E, gavage administration of NSC12 resulted in a significant inhibition of H520 tumor growth that was confirmed by measuring the end-stage tumor weight. This occurred in the absence of any effect of drug administration on body weight and survival of treated animals.

DISCUSSION

Here we demonstrate that *Tie2* promoter-driven hPTX3 overexpression in transgenic mice inhibits tumor growth, angiogenesis, and metastasis in heterotopic, orthotopic, and autochthonous FGF-dependent tumor models. On this basis, pharmacophore modeling of the interaction of the minimal PTX3-derived FGF-binding pentapeptide ARPCA with FGF2 was used for the identification of NSC12 as a small-molecule FGF trap active by parenteral as well as by gavage administration in tumor-bearing mice.

Several pieces of evidence support the hypothesis that the oncosuppressive effects of hPTX3 are due to its capacity to act as a natural FGF trap: (1) the endothelium of TgN(Tie2-hPTX3) mice shows a reduced response to FGF2 in various angiogenesis assays but retains a full capacity to respond to VEGF stimulation; (2) inhibition of FGFR1 phosphorylation occurs in FGF-dependent TRAMP-C2 cells grafted in TgN(Tie2-hPTX3) mice; and (3) hPTX3 expression does not affect the growth of FGF-independent TC-1 or C3 tumors. We cannot rule out the possibility that PTX3 may have multiple impacts on tumor growth (Bonavita et al., 2015). Nevertheless, our data support the notion that the anti-tumor effects of hPTX3 are related to its inhibitory action on the autocrine and paracrine loops of stimulation triggered by the FGF/FGFR system in FGF-dependent tumors, setting the basis for the identification of a PTX3-derived small-molecule FGF trap. Clearly different from FGFR blockers, PTX3 and PTX3-derived FGF traps are anticipated to be ineffective on tumors driven by ligand-independent FGFR activation, as shown for FGFR1-TRAMP-C2 cells grafted in TgN(Tie2-hPTX3) mice.

ARPCA, corresponding to the amino acid sequence PTX3 (100–104), represents the minimal FGF2-binding peptide able to antagonize FGF2 activity by interacting with the FGFR-binding region of the growth factor. These findings provided the bases for the design of a pharmacophore model of ARPCA/FGF2 interaction that was used for in silico screening of the NCI2003 small-molecule database, thus allowing the identification of NSC12 as an ARPCA mimic. As anticipated, NSC12 binds FGF2 with a 1:1 stoichiometry and inhibits the formation of bioactive HSPG/FGF2/FGFR1 ternary complexes by inhibiting FGF2/FGFR interaction with no effect on FGF2/heparin interaction. Also, MD simulation-based studies of the FGF2/ARPCA and FGF2/NSC12 systems indicate that, because of the design process, both molecules may engage the FGF2 surface that faces the FGFR D3 domain and D2-D3 linker. Moreover, NSC12 further extends its interaction into the FGF2 region facing the FGFR D2 domain. Accordingly, NMR relaxation data showed the ability of NSC12 to cause the dissociation of the FGF2/D2 complex. Even though further experiments involving the D2-D3 FGFR domains will be required to fully elucidate the inhibitory mechanism of NSC12, the combined MD, NMR, biochemical, and biological data provide compelling evidence of the ability of the compound to act as an FGF antagonist.

Previous studies had identified the small molecule sm27 as a mimic of the FGF2-binding sequence of thrombospondin-1 able to engage the heparin-binding site of FGF2 (Pagano et al., 2012). As observed for other anionic compounds (Presta et al., 2005), sm27 may interact with the heparin-binding domain of a variety of signaling proteins with possible unsought side effects. In contrast, the action of NSC12 appears to be restricted to FGF family members due to its direct effect on FGF/FGFR interaction with no effect on the heparin-binding VEGF-A_{165} isoform. Accordingly, NSC12 inhibits the proliferation of various FGF-dependent murine and human cancer cell lines with no inhibitory

(E–G) Mice implanted s.c. with alginate plugs containing FGF-dependent human DU145 (E) or H520 (F) cells or FGF-independent human HCC827 (G) cells were treated i.p. every other day with 7.5 mg/Kg NSC12, NSC21, or vehicle for 1 week (n = 4–6 mice/group). Harvested plugs were weighed, and immunofluorescence analysis was performed.

Scale bars, 30 μm (B), 50 μm {E, F, and G [H&E]), and 100 μm (E, F, and G [CD31, TUNEL, and Ki67]). Data are mean ± SEM. In box and whiskers graphs, boxes extend from the 25th to the 75th percentiles, lines indicate the median values, and whiskers indicate the range of values. **$p < 0.01$, #$p < 0.001$, and §$p < 0.05$ versus NSC12 at 2.5 and 5 mg/Kg. See also Figure S5.

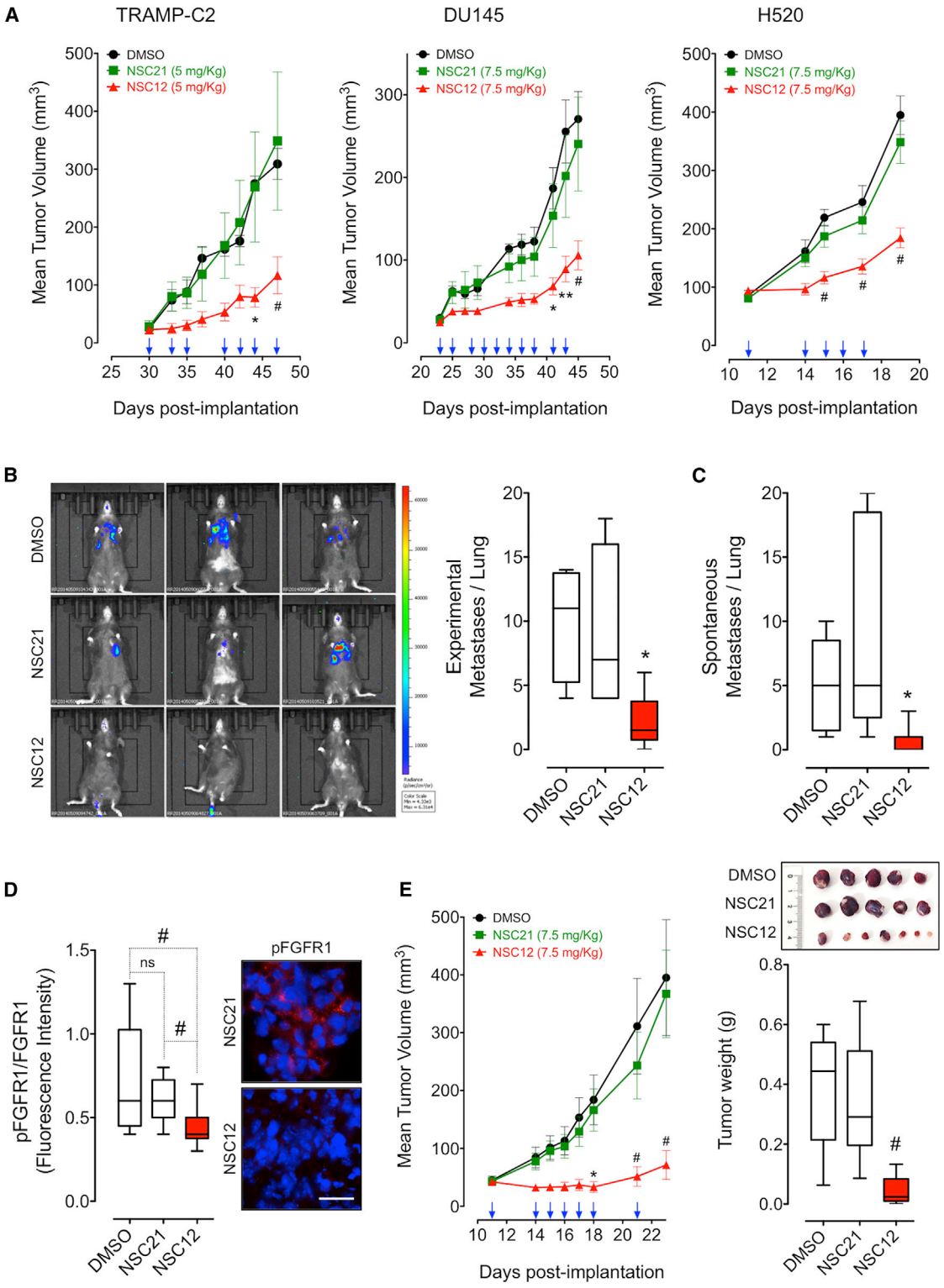

Figure 7. Anti-tumor and Anti-metastatic Activity of NSC12

(A) Growth of s.c. TRAMP-C2, DU145, and H520 tumors in mice treated i.p. (arrows) with NSC12, NSC21, or vehicle (n = 10–16 mice/group).

(B) B16-F10-*luc* cells were injected i.v., and mice were treated i.p. for 2 weeks every other day with NSC12, NSC21, or vehicle (n = 6–8 mice/group). Bioluminescence imaging of lung colonization at day 21 is shown as is count of lung macrometastases at day 28.

(C) Number of spontaneous lung macrometastases 5 weeks after primary EO771 tumor removal and treatment with DMSO, NSC12, or NSC21 (n = 8–10 mice/group).

(legend continued on next page)

effect on HCC827 cancer cells that harbor a tumor-driving mutation of the EGFR TK domain and on FGF-independent cancer cell lines. Thus, NSC12 may act as a selective "two-compartment" epithelial-stromal targeting agent in FGF/FGFR-dependent tumors. Accordingly, i.p. and gavage administration of NSC12 hampers FGFR phosphorylation, angiogenesis, and primary and metastatic growth of FGF-dependent murine and human tumors in mice.

The FGF/FGFR system is implicated in various steps of tumor growth and progression (Beenken and Mohammadi, 2009). In addition, activation of the FGF/FGFR pathway is a mechanism of tumor escape in response to anti-VEGF therapies (Casanovas et al., 2005; Lieu et al., 2011). Thus, FGF blockade may represent a valid therapeutic option for selected tumors driven by an aberrant ligand-dependent FGFR activation (Dieci et al., 2013). However, the development of drugs specifically targeting the FGF/FGFR pathway proved to be difficult, in part due to the high redundancy and pleiotropic effects of FGF and FGFR family members. Blockade of FGFR signaling by selective or broad-spectrum TK inhibitors has been associated with toxicity (Dieci et al., 2013), and a monoclonal antibody directed against FGFR1 has failed because of severe weight loss associated with hypothalamic binding (Sun et al., 2007). On the other hand, an allosteric multi-FGFR blocker with promising therapeutic implications has been described recently (Bono et al., 2013).

Drugs targeting FGF ligands may represent an interesting alternative to FGFR inhibitors. They include monoclonal antibodies and FGFR-derived decoy molecules acting as FGF traps (Harding et al., 2013; Ho et al., 2014). These molecules, however, have various limitations due to their proteinaceous origin. Our data demonstrate that NSC12 interacts with all members of the canonical FGF subfamilies involved in the growth of different human tumors (Ronca et al., 2015). Moreover, NSC12 prevents FGF interaction with all four FGFRs. Thus, NSC12 represents a small-molecule multi-FGF trap with potential implications for cancer therapy. Of note, in keeping with the lack of pathological consequences following constitutive hPTX3 expression in transgenic mice, the anti-tumor action of NSC12 occurred in the absence of any systemic toxic effect in treated animals. In particular, in contrast to the *hyperphosphatemic* effect of FGFR TK inhibitors in preclinical models (Brown et al., 2005) and cancer patients (Dieci et al., 2013), long-term administration of NSC12 did not affect the blood levels of phosphorus, calcium, and FGF23. Moreover, qRT-PCR analysis did not show any change of *Fgf23* expression in kidneys and bone of NSC12-treated mice (data not shown). This occurred despite the capacity of NSC12 to affect the mitogenic activity of hormonal FGFs, including FGF23, when tested on MDA-MB-361 breast cancer cells. These observations are in keeping with the safety profile of the FGFR1-derived FGF trap FP-1039 (Harding et al., 2013) and of the allosteric multi-FGFR blocker SSR128129E (Bono et al., 2013). Together, these findings suggest that hyperphosphatemia may represent a side effect of FGFR TK inhibitors rather than of extracellular inhibitors of the FGF/FGFR system. Given that both *FGF23* expression and activity are under the control of a complex mechanism of regulation that includes canonical, noncanonical, and intracrine FGF/FGFR pathways (Martin et al., 2012; Han et al., 2015), further studies are required to elucidate this point.

Data from phase I and II clinical trials indicate that inhibition of the FGF/FGFR system may show anti-tumor activity and provide an incentive to develop additional safer and more efficacious drugs (Dieci et al., 2013). NSC12 represents a lead compound for the development of orally active small-molecule therapeutics for the treatment of tumors in which the ligand-dependent activation of the FGFR pathway is an oncogenic driver or is involved in the escape to conventional anti-cancer/anti-angiogenic therapies. Finally, from a broader perspective, our data emphasize the possibility to exploit protein interactome for the design of orally active small-molecule multi-ligand traps with promising implications in cancer therapy.

EXPERIMENTAL PROCEDURES

Reagents and Cell Cultures

Reagents, recombinant proteins, and cell line cultures are detailed in the Supplemental Experimental Procedures.

NSC12 Identification

Molecular dynamics simulations of ARPCA and NSC12, generation of a structural ARPCA-FGF2 complex model, pharmacophore model generation, screening process and parameters, and NMR analysis are detailed in the Supplemental Experimental Procedures.

Western Blotting and PCR Analyses

Tissues and tumor lysates were separated by SDS-PAGE and immunodecorated with specific antibodies as described in the Supplemental Experimental Procedures. RT-PCR and qRT-PCR were performed using equal amounts of input RNA and applying specific amplification conditions as detailed in the Supplemental Experimental Procedures.

Surface Plasmon Resonance and CONAMORE

SPR analyses were performed using a BIAcore X-100 apparatus (BIAcore). Experimental conditions for SPR and details for CONAMORE analyses are described in the Supplemental Experimental Procedures.

Angiogenesis Assays

In vitro endothelial cell sprouting, ex vivo murine aorta ring, and in vivo CAM and Matrigel plug assays are described in the Supplemental Experimental Procedures.

Other Assays

Protocols used for cell proliferation, cell-cell adhesion, immunostaining, and other in vitro assays are detailed in the Supplemental Experimental Procedures.

Transgenic Mice

TgN(Tie2-hPTX3) mice were generated via injection of vesicular stomatitis virus G protein (VSV-G)-pseudotyped Tie2-hPTX3 lentiviral particles into

(D) Inhibition of FGFR1 activation in s.c. TRAMP-C2/alginate plugs after 4-day oral treatment with NSC12 (7.5 mg/Kg; 4–6 mice/group). pFGFR1/FGFR1 was quantified and normalized to DAPI area. Scale bar, 30 μm.

(E) Growth of H520 tumors in mice orally treated (arrows) with NSC12, NSC21, or vehicle. At the end of the experiment, harvested tumors were photographed and weighed (n = 10–12 mice/group).

Data are mean ± SEM. In box and whiskers graphs, boxes extend from the 25th to the 75th percentiles, lines indicate the median values, and whiskers indicate the range of values. *p < 0.05, **p < 0.01, #p < 0.001, and ns = not significant. See also Figure S6.

C57BL/6 embryos. Tie2-hPTX3-manipulated embryos were implanted into the oviduct of pseudopregnant CD1 mice, pups were genotyped for the presence of hPTX3 and lentiviral vector backbone, and the transgenic strain was maintained as described in the Supplemental Experimental Procedures. TRAMP mice were purchased from the Jackson Laboratory. Double-transgenic TgN(Tie2-hPTX3)/TRAMP mice were generated by crossing homozygous TRAMP females with Tie2-hPTX3 males.

Animal Experiments

Subcutaneous tumor models were performed by injecting TRAMP-C2 (5×10^6), LLC (5×10^4), and B16-F10 (1×10^4) cells into the flank of C57BL/6 mice; human H520, DU145, and HCC827 cells were injected (5×10^6) into the flank of nude mice. Tumor growth was measured by using calipers, and tumor volume (V) was calculated as follows: $V = (\text{length} \times \text{width}^2) \times 0.5$. For experimental metastasis assays, M5076 (3×10^4) and B16-F10 (1×10^4) cells were injected via the tail vein. Panc02 cells were used for orthotopic tumor growth, and EO771 cells were used for orthotopic and spontaneous metastasis models. Experimental conditions, tumor and metastasis assays, treatments, and all procedures are detailed in the Supplemental Experimental Procedures.

Ethical Regulations

Animal experiments were approved by our local animal ethics committee (OPBA) at the University of Brescia and were executed in accordance with national guidelines and regulations.

Statistical Analyses

Statistical analyses were performed using the statistical package Prism 5 (GraphPad Software) as detailed in the Supplemental Experimental Procedures. Differences were considered significant with $p < 0.05$.

SUPPLEMENTAL INFORMATION

Supplemental Information includes Supplemental Experimental Procedures and six figures and can be found with this article online at http://dx.doi.org/10.1016/j.ccell.2015.07.002.

AUTHOR CONTRIBUTIONS

R.R. conceived in vivo experiments, generated mice, and analyzed the data. A.G. conceived in vitro experiments, analyzed the data, and revised the manuscript. S.R. performed animal experiments. A.G., E.D.S., and S.M. performed in vitro and SPR studies. A.G. and D.C. performed histological analyses. K.P. and L.R. performed NMR studies. D.M. performed CONAMORE studies. R.T., E.M., and G.C. generated the pharmacophore model and performed MD studies. R.M. and G.E. provided lentiviral vectors. M.M. synthetized NSC12. R.R. and M.P. wrote the manuscript.

ACKNOWLEDGMENTS

This work was supported by grants from Ministero Istruzione, Università e Ricerca (FIRB project RBAP11H2R9 2011), Associazione Italiana Ricerca sul Cancro (AIRC grant 14395) to M.P., and AIRC grant IG 15420 and Fondazione Cariplo (grant 2011.1800 "Premio Fondazione Cariplo per la Ricerca di Frontiera") to G.C. A.G. and S.M. were supported by Fondazione Italiana per la Ricerca sul Cancro fellowships, E.D.S. by a Fondazione Veronesi fellowship, and K.P. by a Fondazione Antonio De Marco grant. NSC compounds were from Drug Synthesis and Chemistry Branch, Developmental Therapeutics Program, Division of Cancer Treatment and Diagnosis, National Cancer Institute (USA). The authors are grateful to C. Garlanda for providing *Ptx3*$^{-/-}$ mice; B. Bottazzi, D. Moi, M. De Palma, L. Zetta, and P. Bergese for helpful discussion and criticisms; and M. Belleri, M. Corsini, A. Bugatti, and D. Leali for technical support.

Received: July 31, 2014
Revised: April 10, 2015
Accepted: July 10, 2015
Published: August 10, 2015

REFERENCES

Accardi, L., Paolini, F., Mandarino, A., Percario, Z., Di Bonito, P., Di Carlo, V., Affabris, E., Giorgi, C., Amici, C., and Venuti, A. (2014). In vivo antitumor effect of an intracellular single-chain antibody fragment against the E7 oncoprotein of human papillomavirus 16. Int. J. Cancer *134*, 2742–2747.

Bai, A., Meetze, K., Vo, N.Y., Kollipara, S., Mazsa, E.K., Winston, W.M., Weiler, S., Poling, L.L., Chen, T., Ismail, N.S., et al. (2010). GP369, an FGFR2-IIIb-specific antibody, exhibits potent antitumor activity against human cancers driven by activated FGFR2 signaling. Cancer Res. *70*, 7630–7639.

Beenken, A., and Mohammadi, M. (2009). The FGF family: biology, pathophysiology and therapy. Nat. Rev. Drug Discov. *8*, 235–253.

Bonavita, E., Gentile, S., Rubino, M., Maina, V., Papait, R., Kunderfranco, P., Greco, C., Feruglio, F., Molgora, M., Laface, I., et al. (2015). PTX3 is an extrinsic oncosuppressor regulating complement-dependent inflammation in cancer. Cell *160*, 700–714.

Bono, F., De Smet, F., Herbert, C., De Bock, K., Georgiadou, M., Fons, P., Tjwa, M., Alcouffe, C., Ny, A., Bianciotto, M., et al. (2013). Inhibition of tumor angiogenesis and growth by a small-molecule multi-FGF receptor blocker with allosteric properties. Cancer Cell *23*, 477–488.

Brooks, A.N., Kilgour, E., and Smith, P.D. (2012). Molecular pathways: fibroblast growth factor signaling: a new therapeutic opportunity in cancer. Clin. Cancer Res. *18*, 1855–1862.

Brown, A.P., Courtney, C.L., King, L.M., Groom, S.C., and Graziano, M.J. (2005). Cartilage dysplasia and tissue mineralization in the rat following administration of a FGF receptor tyrosine kinase inhibitor. Toxicol. Pathol. *33*, 449–455.

Camozzi, M., Rusnati, M., Bugatti, A., Bottazzi, B., Mantovani, A., Bastone, A., Inforzato, A., Vincenti, S., Bracci, L., Mastroianni, D., and Presta, M. (2006). Identification of an antiangiogenic FGF2-binding site in the N terminus of the soluble pattern recognition receptor PTX3. J. Biol. Chem. *281*, 22605–22613.

Casanovas, O., Hicklin, D.J., Bergers, G., and Hanahan, D. (2005). Drug resistance by evasion of antiangiogenic targeting of VEGF signaling in late-stage pancreatic islet tumors. Cancer Cell *8*, 299–309.

Colombo, G., Margosio, B., Ragona, L., Neves, M., Bonifacio, S., Annis, D.S., Stravalaci, M., Tomaselli, S., Giavazzi, R., Rusnati, M., et al. (2010). Non-peptidic thrombospondin-1 mimics as fibroblast growth factor-2 inhibitors: an integrated strategy for the development of new antiangiogenic compounds. J. Biol. Chem. *285*, 8733–8742.

Daigo, K., Mantovani, A., and Bottazzi, B. (2014). The yin-yang of long pentraxin PTX3 in inflammation and immunity. Immunol. Lett. *161*, 38–43.

De Palma, M., Murdoch, C., Venneri, M.A., Naldini, L., and Lewis, C.E. (2007). Tie2-expressing monocytes: regulation of tumor angiogenesis and therapeutic implications. Trends Immunol. *28*, 519–524.

Dieci, M.V., Arnedos, M., Andre, F., and Soria, J.C. (2013). Fibroblast growth factor receptor inhibitors as a cancer treatment: from a biologic rationale to medical perspectives. Cancer Discov. *3*, 264–279.

Garlanda, C., Bottazzi, B., Bastone, A., and Mantovani, A. (2005). Pentraxins at the crossroads between innate immunity, inflammation, matrix deposition, and female fertility. Annu. Rev. Immunol. *23*, 337–366.

Giacomini, A., Matarazzo, S., Pagano, K., Ragona, L., Rezzola, S., Corsini, M., Di Salle, E., Presta, M., and Ronca, R. (2015). A long pentraxin-3-derived pentapeptide for the therapy of FGF8b-driven steroid hormone-regulated cancers. Oncotarget *6*, 13790–13802.

Han, X., Xiao, Z., and Quarles, L.D. (2015). Membrane and integrative nuclear fibroblastic growth factor receptor (FGFR) regulation of FGF-23. J. Biol. Chem. *290*, 10447–10459.

Harding, T.C., Long, L., Palencia, S., Zhang, H., Sadra, A., Hestir, K., Patil, N., Levin, A., Hsu, A.W., Charych, D., et al. (2013). Blockade of nonhormonal fibroblast growth factors by FP-1039 inhibits growth of multiple types of cancer. Sci. Transl. Med. *5*, 178ra39.

Hart, K.C., Robertson, S.C., Kanemitsu, M.Y., Meyer, A.N., Tynan, J.A., and Donoghue, D.J. (2000). Transformation and Stat activation by derivatives of FGFR1, FGFR3, and FGFR4. Oncogene *19*, 3309–3320.

Herbert, C., Schieborr, U., Saxena, K., Juraszek, J., De Smet, F., Alcouffe, C., Bianciotto, M., Saladino, G., Sibrac, D., Kudlinzki, D., et al. (2013). Molecular mechanism of SSR128129E, an extracellularly acting, small-molecule, allosteric inhibitor of FGF receptor signaling. Cancer Cell *23*, 489–501.

Ho, H.K., Yeo, A.H., Kang, T.S., and Chua, B.T. (2014). Current strategies for inhibiting FGFR activities in clinical applications: opportunities, challenges and toxicological considerations. Drug Discov. Today *19*, 51–62.

Inforzato, A., Baldock, C., Jowitt, T.A., Holmes, D.F., Lindstedt, R., Marcellini, M., Rivieccio, V., Briggs, D.C., Kadler, K.E., Verdoliva, A., et al. (2010). The angiogenic inhibitor long pentraxin PTX3 forms an asymmetric octamer with two binding sites for FGF2. J. Biol. Chem. *285*, 17681–17692.

Itoh, N., and Ornitz, D.M. (2004). Evolution of the Fgf and Fgfr gene families. Trends Genet. *20*, 563–569.

Leali, D., Bianchi, R., Bugatti, A., Nicoli, S., Mitola, S., Ragona, L., Tomaselli, S., Gallo, G., Catello, S., Rivieccio, V., et al. (2010). Fibroblast growth factor 2-antagonist activity of a long-pentraxin 3-derived anti-angiogenic pentapeptide. J. Cell. Mol. Med. *14*, 2109–2121.

Leali, D., Alessi, P., Coltrini, D., Ronca, R., Corsini, M., Nardo, G., Indraccolo, S., and Presta, M. (2011). Long pentraxin-3 inhibits FGF8b-dependent angiogenesis and growth of steroid hormone-regulated tumors. Mol. Cancer Ther. *10*, 1600–1610.

Leali, D., Inforzato, A., Ronca, R., Bianchi, R., Belleri, M., Coltrini, D., Di Salle, E., Sironi, M., Norata, G.D., Bottazzi, B., et al. (2012). Long pentraxin 3/tumor necrosis factor-stimulated gene-6 interaction: a biological rheostat for fibroblast growth factor 2-mediated angiogenesis. Arterioscler. Thromb. Vasc. Biol. *32*, 696–703.

Lieu, C., Heymach, J., Overman, M., Tran, H., and Kopetz, S. (2011). Beyond VEGF: inhibition of the fibroblast growth factor pathway and antiangiogenesis. Clin. Cancer Res. *17*, 6130–6139.

Maiolo, D., Mitola, S., Leali, D., Oliviero, G., Ravelli, C., Bugatti, A., Depero, L.E., Presta, M., and Bergese, P. (2012). Role of nanomechanics in canonical and noncanonical pro-angiogenic ligand/VEGF receptor-2 activation. J. Am. Chem. Soc. *134*, 14573–14579.

Martin, A., David, V., and Quarles, L.D. (2012). Regulation and function of the FGF23/klotho endocrine pathways. Physiol. Rev. *92*, 131–155.

Pagano, K., Torella, R., Foglieni, C., Bugatti, A., Tomaselli, S., Zetta, L., Presta, M., Rusnati, M., Taraboletti, G., Colombo, G., and Ragona, L. (2012). Direct and allosteric inhibition of the FGF2/HSPGs/FGFR1 ternary complex formation by an antiangiogenic, thrombospondin-1-mimic small molecule. PLoS ONE *7*, e36990.

Plotnikov, A.N., Schlessinger, J., Hubbard, S.R., and Mohammadi, M. (1999). Structural basis for FGF receptor dimerization and activation. Cell *98*, 641–650.

Polnaszek, N., Kwabi-Addo, B., Peterson, L.E., Ozen, M., Greenberg, N.M., Ortega, S., Basilico, C., and Ittmann, M. (2003). Fibroblast growth factor 2 promotes tumor progression in an autochthonous mouse model of prostate cancer. Cancer Res. *63*, 5754–5760.

Presta, M., Oreste, P., Zoppetti, G., Belleri, M., Tanghetti, E., Leali, D., Urbinati, C., Bugatti, A., Ronca, R., Nicoli, S., et al. (2005). Antiangiogenic activity of semisynthetic biotechnological heparins: low-molecular-weight-sulfated Escherichia coli K5 polysaccharide derivatives as fibroblast growth factor antagonists. Arterioscler. Thromb. Vasc. Biol. *25*, 71–76.

Presta, M., Camozzi, M., Salvatori, G., and Rusnati, M. (2007). Role of the soluble pattern recognition receptor PTX3 in vascular biology. J. Cell. Mol. Med. *11*, 723–738.

Richard, C., Liuzzo, J.P., and Moscatelli, D. (1995). Fibroblast growth factor-2 can mediate cell attachment by linking receptors and heparan sulfate proteoglycans on neighboring cells. J. Biol. Chem. *270*, 24188–24196.

Ronca, R., Alessi, P., Coltrini, D., Di Salle, E., Giacomini, A., Leali, D., Corsini, M., Belleri, M., Tobia, C., Garlanda, C., et al. (2013a). Long pentraxin-3 as an epithelial-stromal fibroblast growth factor-targeting inhibitor in prostate cancer. J. Pathol. *230*, 228–238.

Ronca, R., Di Salle, E., Giacomini, A., Leali, D., Alessi, P., Coltrini, D., Ravelli, C., Matarazzo, S., Ribatti, D., Vermi, W., and Presta, M. (2013b). Long pentraxin-3 inhibits epithelial-mesenchymal transition in melanoma cells. Mol. Cancer Ther. *12*, 2760–2771.

Ronca, R., Giacomini, A., Rusnati, M., and Presta, M. (2015). The potential of fibroblast growth factor/fibroblast growth factor receptor signaling as a therapeutic target in tumor angiogenesis. Expert Opin. Ther. Targets, 1–17.

Shojaei, F., Wu, X., Qu, X., Kowanetz, M., Yu, L., Tan, M., Meng, Y.G., and Ferrara, N. (2009). G-CSF-initiated myeloid cell mobilization and angiogenesis mediate tumor refractoriness to anti-VEGF therapy in mouse models. Proc. Natl. Acad. Sci. USA *106*, 6742–6747.

Sun, H.D., Malabunga, M., Tonra, J.R., DiRenzo, R., Carrick, F.E., Zheng, H., Berthoud, H.R., McGuinness, O.P., Shen, J., Bohlen, P., et al. (2007). Monoclonal antibody antagonists of hypothalamic FGFR1 cause potent but reversible hypophagia and weight loss in rodents and monkeys. Am. J. Physiol. Endocrinol. Metab. *292*, E964–E976.

Talmadge, J.E., and Hart, I.R. (1984). Inhibited growth of a reticulum cell sarcoma (M5076) induced in vitro and in vivo by macrophage-activating agents. Cancer Res. *44*, 2446–2451.

Urakawa, I., Yamazaki, Y., Shimada, T., Iijima, K., Hasegawa, H., Okawa, K., Fujita, T., Fukumoto, S., and Yamashita, T. (2006). Klotho converts canonical FGF receptor into a specific receptor for FGF23. Nature *444*, 770–774.

Zhang, X., Ibrahimi, O.A., Olsen, S.K., Umemori, H., Mohammadi, M., and Ornitz, D.M. (2006). Receptor specificity of the fibroblast growth factor family. The complete mammalian FGF family. J. Biol. Chem. *281*, 15694–15700.